






Article

Reconstructing Reliable Powder Patterns from Spikelets (Q)CPMG NMR Spectra: Simplification of UWNMR Crystallography Analysis

Andrii Mahun ^{1,2}, Sabina Abbrent ¹, Jiri Czernek ¹, Jan Rohlicek ³, Hana Macková ¹, Weihua Ning ^{4,†}, Rafal Konefal ¹, Jiří Brus ¹ and Libor Kobera ^{1,*}

¹ Institute of Macromolecular Chemistry of the Czech Academy of Sciences, Heyrovskeho nam. 2, 162 06 Prague 6, Czech Republic; mahun@imc.cas.cz (A.M.); abbrent@imc.cas.cz (S.A.); czernek@imc.cas.cz (J.C.); mackova@imc.cas.cz (H.M.); konefal@imc.cas.cz (R.K.); brus@imc.cas.cz (J.B.)

² Department of Physical and Macromolecular Chemistry, Faculty of Science, Charles University, Hlavova 8, 128 40 Prague 2, Czech Republic

³ Department of Structural Analysis, Institute of Physics of the Czech Academy of Sciences, Na Slovance 2, 182 21 Prague 8, Czech Republic; rohlicek@fzu.cz

⁴ Department of Physics, Chemistry and Biology (IFM), Linköping University, SE-581 83 Linköping, Sweden; weihua.ning@liu.se

* Correspondence: kobera@imc.cas.cz

† Current address: Institute of Functional Nano & Soft Materials (FUNSOM), Jiangsu Key Laboratory for Carbon-Based Functional Materials & Devices, Soochow University, Suzhou 215123, China.



Citation: Mahun, A.; Abbrent, S.; Czernek, J.; Rohlicek, J.; Macková, H.; Ning, W.; Konefal, R.; Brus, J.; Kobera, L. Reconstructing Reliable Powder Patterns from Spikelets (Q)CPMG NMR Spectra: Simplification of UWNMR Crystallography Analysis. *Molecules* **2021**, *26*, 6051. <https://doi.org/10.3390/molecules26196051>

Academic Editor: Dorota Flak

Received: 8 September 2021

Accepted: 30 September 2021

Published: 6 October 2021

Publisher's Note: MDPI stays neutral with regard to jurisdictional claims in published maps and institutional affiliations.



Copyright: © 2021 by the authors. Licensee MDPI, Basel, Switzerland. This article is an open access article distributed under the terms and conditions of the Creative Commons Attribution (CC BY) license (<https://creativecommons.org/licenses/by/4.0/>).

Abstract: Spikelets NMR spectra are very popular as they enable the shortening of experimental time and give the possibility to obtain required NMR parameters for nuclei with ultrawide NMR patterns. Unfortunately, these resulted ssNMR spectra cannot be fitted directly in common software. For this reason, we developed UWNMRsSpectralShape (USS) software which transforms spikelets NMR patterns into single continuous lines. Subsequently, these reconstructed spectral envelopes of the (Q)CPMG spikelets patterns can be loaded into common NMR software and automatically fitted, independently of experimental settings. This allows the quadrupole and chemical shift parameters to be accurately determined. Moreover, it makes fitting of spikelets NMR spectra exact, fast and straightforward.

Keywords: UWNMR; spikelets NMR spectra; NMR software; spectral envelope

1. Introduction

In the last fifty years, NMR spectroscopy has undergone progressive development. One of the first NMR publications sixty years ago opened the door for NMR studies, providing valuable information about the molecular structure and dynamics in solid systems [1]. Almost simultaneously, the classic paper “*Nuclear Electric Quadrupolar Interactions in Crystals*” was published by R. V. Pound [2], and, over the next few years, many papers dealing with the analysis of quadrupolar NMR powder lineshapes were published. Since ca. 75% of NMR active nuclei have a quadrupolar character (spin $I > 1/2$) and, therefore, provide very broad and complicated spectral lines, this area is still under scrutiny. Many of these quadrupolar nuclei are unreceptive to the traditional NMR experiments due to their low natural abundance or low gyromagnetic ratio. Moreover, additional complications arise from the anisotropic broadening of powder patterns which dramatically reduce the signal-to-noise ratio (SNR). As the resulting powder patterns can reach from tens kHz to a few MHz in width, they cannot be acquired using techniques such as the single-pulsed (SP) experiment because of the inability to efficiently excite the whole powder pattern, signal loss during the ring-down of the probe and the recovery of the receiver immediately after the pulse. The description of dominant anisotropic NMR interactions is necessary for the

understanding of quadrupolar nuclei behavior such as (i) the quadrupolar interaction [3], (ii) chemical shift/chemical shift anisotropy [4] or (iii) anisotropic broadening induced by the presence of unpaired electrons [5]. Residual interactions, such as dipolar and scalar interactions, can be, in this case, omitted due to their relatively low values.

Quadrupolar interaction exists between local electric field gradients (EFGs) and the nuclear quadrupolar moment (Q). The traceless and symmetric local EFG tensor is defined as $|V_{33}| \geq |V_{22}| \geq |V_{11}|$. The quadrupolar coupling constant— C_Q —and the asymmetry parameter— η_Q —are derived from the principal values of the EFG tensor ($V_{33} = eq$) as follows: $C_Q = e^2qQ/h$ and $\eta_Q = (V_{11} - V_{22})/V_{33}$. These two parameters define the quadrupolar interaction and can be extracted from recorded NMR powder patterns. They allow an insight into spherical and axial symmetry of the local electronic environment. In recent decades, many experimental techniques have been developed enabling the acquisition of quadrupolar parameters (i.e., DOR [6], DAS [7], STMAS [8,9], MQMAS [10]). However, most of these techniques can only be used for patterns narrower than 150 kHz in breadth. For wider spectral lines, usually defined as Ultra-Wideline NMR patterns [11–13] (UWNMR), special NMR techniques based on piecewise spectral acquisition [14–16] or spin echo [17] have to be applied. The term “piecewise technique” is used when the full pattern is obtained by conducting and co-adding a series of experiments where each provides a section of individual points or sub-spectra. This technique uses two possible approaches: (i) field stepping, where the transmitter frequency is constant and the magnetic field is incremented or (ii) frequency stepping, where the transmitter frequency is incremented at a constant magnetic field. While these techniques provide valuable results and are used to this day, the weaker spectral resolution and extensive experimental time represent their undismissible disadvantage.

On the other hand, “spin echo techniques”, originally proposed by Hahn [17] and composed of two pulses with an inserted delay ($90^\circ\text{-}\tau\text{-}180^\circ\text{-}aq.$), are designed for the effective refocusing of dephased spins and to provide spectral lines with a sufficient resolution. A modified technique known as quadrupolar or solid echo, commonly used for measurements of quadrupolar nuclei, uses shorter pulses, (i.e., $90^\circ\text{-}\tau\text{-}90^\circ\text{-}aq$) [18,19]. In the case of UWNMR, the spin echo approach can be used in combination with the frequency stepping technique and called “variable-offset cumulative spectroscopy” (VOCS) [16]. Furthermore, the “Hahn echo” approach was further extended by Carr and Purcell for measurements of T_2 relaxation times (the second delay was spaced between the second pulse and acquisition time $90^\circ\text{-}\tau\text{-}180^\circ\text{-}\tau\text{-}aq.$) [20]. Subsequently, Meiboom and Gill modified the Carr–Purcell sequence, adding a train of 180° pulses with a 90° phase shift with respect to the first pulse ($90^\circ\text{-}\tau\text{-}(180^\circ\text{-}\tau\text{-}aq.)_n$) [21]. The resulting Carr–Purcell–Meiboom–Gill (CPMG) sequence is a suitable tool for the enhancement of SNR of solid-state NMR (ssNMR) spectra. Later, pioneering work was presented by Sinfelt for nuclei with spin $I = 1/2$ [22]. Twenty years ago, Larsen used the CPMG sequence for quadrupolar nuclei (QCPMG) [23] and a further combination with the frequency-stepped experiment allowed the recording of UWNMR spectra with satisfactory SNR [24]. Then, each echo-train was recorded as a single FID and was Fourier-transformed as an entity and then combined into a “spikelets” spectrum. However, obtaining UWNMR spectra in one piece was still a challenge and, therefore, an alternative approach was developed which applies constant transmitter frequencies with the modulation of either pulse amplitude or phase in order to excite a broad enough frequency range. In 2007, Bhattacharyya and Frydman replaced the regular pulses in the Hahn echo with an adiabatic sequence [25] termed “wide-band, uniform-rate, and smooth truncation” (WURST) introduced by Kupce and Freeman in 1995 for the uniform excitation of a broad frequency range, [26] resulting in the so-called WURST-echo sequence [27]. Subsequently, Schurko et al. published the WURST-QCPMG sequence where all pulses were substituted by WURST-80 pulses [28]. This approach allows acquiring UWNMR spectra in one piece that would normally require frequency-stepped (VOCS) techniques. Finally, Schurko et al. successfully applied this approach to various spin- $1/2$ nuclei (i.e., ^{119}Sn , ^{195}Pt , ^{199}Hg and ^{207}Pb), which are known to exhibit strong CSA

interactions, making it difficult to obtain the powder pattern by frequently used techniques (SP/MAS, MQ/MAS, etc.) [29].

Usually, required NMR parameters (quadrupolar parameters (C_Q , η_Q) and chemical shift anisotropy (CSA), etc.) are extracted from resulting (Q)CPMG spectra using a careful manual simulation and fitting of the powder pattern. This approach is relatively time-consuming and should be supported by data obtained from quantum chemical calculations. Here, another complication arises as an agreement between calculated data and experimental data is not always guaranteed.

Therefore, we developed a tool for the easy extraction of the spectral envelopes of the obtained spikelets powder pattern from (Q)CPMG NMR spectra, which can be used for the automatic fitting procedure. The outcome of this automated procedure is an accurate spectral envelope of the UWNMR pattern that can be easily used for the extraction of valuable NMR parameters. The developed software was verified using materials with a known structure and NMR parameters. Additionally, the developed approach was compared with the existing method for obtaining spectral envelopes by (time-domain) the co-addition of individual spin echoes followed by a Fourier transformation (FFT). As a final step, unknown NMR parameters were successfully extracted from reconstructed newly obtained single continuous spectral lines and confirmed by DFT calculations.

2. Results and Discussion

2.1. Verification of the USS Software Using Model Spectra

For the validation and verification of reconstructed spectral envelopes obtained using USS software, a diverse group of NMR active nuclei was selected. Both quadrupolar (^{137}Ba , ^{35}Cl and ^{27}Al) and spin- $1/2$ nuclei (^{207}Pb and ^{199}Hg) were chosen and experimental WURST-(Q)CPMG NMR spikelets spectra of $\text{Ba}(\text{NO}_3)_2$, BaCO_3 , $\text{BaCl}_2 \cdot 2\text{H}_2\text{O}$, $\text{AlMe}_3 + \text{AlMe}_3 \cdot \text{THF}$, $\text{Pb}(\text{HCOO})_2$ and $\text{Hg}(\text{CH}_3\text{COO})_2$, with known structures and NMR parameters were acquired (see Figure 1, expt.). These model compounds possess various structural features, allowing us to demonstrate wide possibilities of this approach. These chosen features were as follows: (i) quadrupolar nuclei with one crystallographic site ($\text{Ba}(\text{NO}_3)_2$ and BaCO_3) but with different quadrupolar coupling constants; (ii) quadrupolar nuclei with two crystallographically different sites ($\text{BaCl}_2 \cdot 2\text{H}_2\text{O}$) of one investigated nucleus; (iii) quadrupolar nuclei containing two distinct crystalline compounds ($\text{AlMe}_3 + \text{AlMe}_3 \cdot \text{THF}$); (iv) spin- $1/2$ nuclei with the dominant contribution of CSA ($\text{Pb}(\text{HCOO})_2$ and $\text{Hg}(\text{CH}_3\text{COO})_2$).

The set of obtained spectra was successfully processed by the USS software, and the final spectral lines were obtained (Figure 1, envelope). In the case of the ^{137}Ba WURST-QCPMG NMR spectrum of BaCO_3 , artifact interferences were observed (Figure 1b; see full spectrum Figure S1). Similarly, in the ^{27}Al WURST-QCPMG NMR spectrum of the $\text{AlMe}_3 + \text{AlMe}_3 \cdot \text{THF}$ sample, the impurities gave additional signals (Figure 1d). Therefore, the structure of BaCO_3 was also confirmed by the XRPD analysis (Figure S2), and a corresponding XRPD pattern of $\text{AlMe}_3 + \text{AlMe}_3 \cdot \text{THF}$ is described in [30].

As the next step, these spectra were transferred to two commonly used programs for NMR data processing (Bruker TopSpin and DMfit). The fitting of the spectral lines was easily accomplished using an automatic procedure and corresponding NMR parameters were obtained. These fittings of spectral lines (Figure 1, TS and DMfit) were in good agreement with the literature data (Figure 1, lit. data). The comparison of experimental and literature-based NMR parameters is listed in Table 1, showing only small differences within the experimental error.

It has been shown [11,31] that the envelope of (Q)CPMG spikelets spectra can be obtained by the summation of individual spin echo FIDs and the subsequent Fourier transformation. The envelopes (of selected compounds) obtained by the co-addition of Fourier-transformed spin echo FIDs were compared with envelopes reconstructed from the USS software, see Figure 2. Clearly, both approaches provided basically the same spectral profiles and the fitted NMR parameters (Table S4) were in great consistency. However, as

the USS software built the spectral envelopes from the maximum points (maxima were also taken from the noise regions), this resulted in a higher SNR, Figure 2, caused by the magnitude processing ('mc' command in TopSpin software) of the spikelets NMR spectra. Although spectral envelopes can be obtained by the above-mentioned spin echo co-addition method, the developed approach (using USS software) was both (i) time-saving and (ii) easy to use. Obtaining the spectral profile by the summation of spin echo requires complicated manipulation with raw data (separation of the initial FID into a set of individual spin echoes with a subsequent FFT procedure of each and manual co-addition of the single spectra into the sum envelope). On the other hand, the USS software provided a fast and intuitive way to generate a spectral envelope without any manipulations with raw data (only a few clicks after loading a spikelets spectrum were needed to obtain the spectral envelope). The developed approach was especially beneficial in the case of UWNMR spikelets spectra obtained by the VOCS technique, since such spectra comprise of tens, in extreme cases hundreds, of sub-spectra.

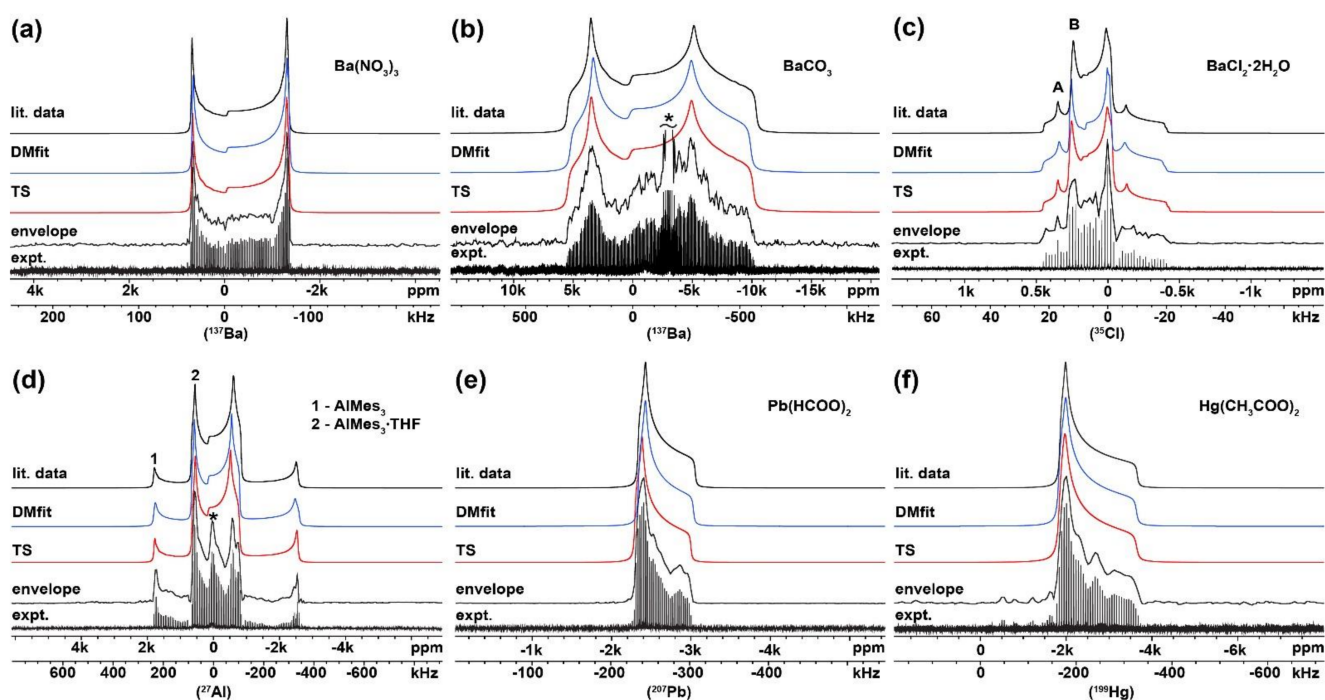


Figure 1. Experimental spikelets WURST-(Q)CPMG NMR spectra (expt.), envelope of the spikelets spectra defined by developed software (envelope), fitting obtained from Bruker TopSpin (TS) and DMfit (DMfit) software, and simulation based on literature data (lit. data) of: (a) ^{137}Ba $\text{Ba}(\text{NO}_3)_2$; (b) ^{137}Ba BaCO_3 ; (c) ^{35}Cl $\text{BaCl}_2 \cdot 2\text{H}_2\text{O}$; (d, 1) ^{27}Al AlMe_3 ; (d, 2) ^{27}Al $\text{AlMe}_3 \cdot \text{THF}$; (e) ^{207}Pb $\text{Pb}(\text{HCOO})_2$; (f) ^{199}Hg $\text{Hg}(\text{CH}_3\text{COO})_2$. Impurities are denoted by asterisk (*).

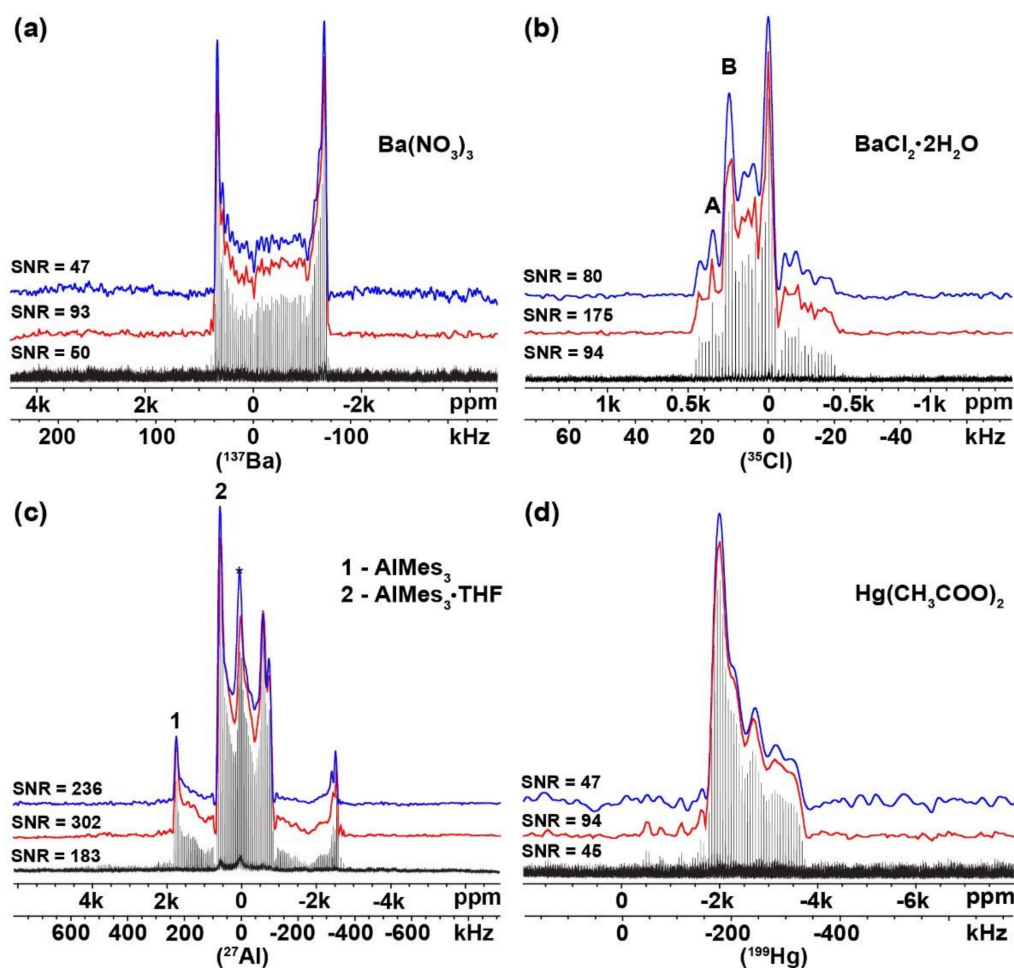


Figure 2. Experimental spikelets WURST(Q)CPMG NMR spectra (black line), spectral profile of the powder pattern obtained by USS software (red line) and co-addition of spin echoes followed by Fourier transformation (blue line) of: (a) (^{137}Ba) $\text{Ba}(\text{NO}_3)_2$; (b) (^{35}Cl) $\text{BaCl}_2 \cdot 2\text{H}_2\text{O}$; (c, 1) (^{27}Al) AlMe_3 ; (c, 2) (^{27}Al) $\text{AlMe}_3 \cdot \text{THF}$; (d) (^{199}Hg) $\text{Hg}(\text{CH}_3\text{COO})_2$.

Table 1. Comparison of experimental NMR parameters with literature data for chosen model compounds.

Compound	Investigated Nuclei	δ_{iso} (ppm)	C_Q (MHz)	η_Q	Ω (ppm)	κ	α (deg)	β (deg)	γ (deg)	Ref.
$\text{Ba}(\text{NO}_3)_2$	^{137}Ba	−42 (8)	7.0 (0.10)	0.01 (0.01)	25 (20)	0.80 (0.20)	40 (20)	10 (25)	—	[32]
		−49 (5)	6.9 (0.10)	0.02 (0.01)	26 (15)	0.80 (0.20)	43 (15)	11 (20)	—	this work ¹
		−47 (5)	6.9 (0.10)	0.02 (0.01)	24 (15)	0.70 (0.20)	53 (20)	32 (20)	—	this work ²
BaCO_3	^{137}Ba	50 (200)	17.4 (0.60)	0.33 (0.04)	150 (150)	0.50 (0.50)	—	—	—	[32]
		76 (150)	16.8 (0.50)	0.34 (0.03)	149 (130)	0.50 (0.40)	—	—	—	this work ¹
		108 (150)	16.6 (0.50)	0.34 (0.03)	183 (140)	0.40 (0.40)	—	—	—	this work ²
$\text{BaCl}_2 \cdot 2\text{H}_2\text{O}$	^{35}Cl (site A)	163 (2)	2.19 (0.08)	0	50 (25)	−0.80 (0.20)	85 (20)	32 (10)	60 (20)	[33]
		167 (10)	2.27 (0.12)	0	39 (25)	−0.60 (0.20)	89 (20)	47 (15)	49 (20)	This work ¹
		164 (10)	2.20 (0.12)	0	43 (25)	−0.60 (0.20)	100 (25)	30 (15)	66 (20)	This work ²
$\text{BaCl}_2 \cdot 2\text{H}_2\text{O}$	^{35}Cl (site B)	156 (2)	3.42 (0.08)	0.30 (0.10)	50 (25)	0.20 (0.25)	20 (15)	8 (10)	0 (20)	[33]
		154 (10)	3.48 (0.15)	0.30 (0.10)	52 (25)	0.20 (0.20)	22 (15)	12 (10)	0 (25)	This work ¹
		158 (10)	3.49 (0.15)	0.30 (0.10)	47 (25)	0.10 (0.20)	15 (15)	15 (10)	5 (25)	This work ²
AlMe_3	^{27}Al (1)	240 (20)	49.2 (0.50)	0.01 (0.01)	126 (10)	−0.99 (0.20)	180 (20)	0 (10)	100 (10)	[30,34]
		242 (15)	49.2 (0.50)	0.01 (0.01)	126 (10)	−0.99 (0.20)	170 (15)	0 (10)	110 (10)	this work ¹
		226 (15)	48.8 (0.50)	0.01 (0.01)	118 (10)	−0.99 (0.20)	180 (15)	0 (10)	100 (10)	this work ²
$\text{AlMe}_3 \cdot \text{THF}$	^{27}Al (2)	120 (10)	27.3 (0.30)	0.13 (0.10)	46 (5)	0.05 (0.10)	205 (10)	80 (5)	200 (10)	[30]
		130 (10)	27.0 (0.30)	0.17 (0.08)	47 (5)	0.05 (0.08)	195 (10)	83 (5)	210 (10)	this work ¹
		133 (10)	26.8 (0.30)	0.17 (0.08)	51 (5)	0.07 (0.08)	200 (10)	80 (5)	215 (15)	this work ²

Table 1. Cont.

Compound	Investigated Nuclei	δ_{iso} (ppm)	C_Q (MHz)	η_Q	Ω (ppm)	κ	α (deg)	β (deg)	γ (deg)	Ref.
Pb (HCOO) ₂	²⁰⁷ Pb	−2567 (20)	—	—	720 (20)	0.75 (0.10)	—	—	—	[35]
		−2562 (15)	—	—	708 (15)	0.74 (0.10)	—	—	—	this work ¹
		−2562 (15)	—	—	701 (20)	0.75 (0.10)	—	—	—	this work ²
Hg (CH ₃ COO) ₂	¹⁹⁹ Hg	−2513 (34)	—	—	1810 (68)	0.89 (0.07)	—	—	—	[29]
		−2485 (40)	—	—	1814 (65)	0.82 (0.07)	—	—	—	this work ¹
		−2488 (40)	—	—	1811 (60)	0.82 (0.07)	—	—	—	this work ²

$\delta_{iso} = (\delta_{11} + \delta_{22} + \delta_{33})/3$, $C_Q = eQV_{33}/h$, $\eta_Q = (V_{11} - V_{22})/V_{33}$, $\Omega = \delta_{11} - \delta_{33}$, $\kappa = 3(\delta_{22} - \delta_{iso})/\Omega$; Euler angles are defined in [36]; ¹ NMR parameters obtained using Bruker TopSpin software; ² NMR parameters obtained using DMfit software.

2.2. Investigation of Compounds with Unknown NMR Parameters

As the developed UWNMR Spectral Shape software was validated on compounds with known NMR parameters, the next step was to use it for extracting unknown NMR parameters. Experimental ⁷¹Ga, ²⁰⁹Bi and ¹¹⁵In WURST-QCPMG NMR spikelets spectra (Figure 3, expt.) of compounds with unknown NMR parameters were recorded and continuous lines obtained using the developed USS software. Subsequently, the spectral envelopes with a small C_Q value were fitted only in the TopSpin software, while the spectral envelopes with a dominant C_Q contribution were fitted in the TopSpin as well as in DMfit software.

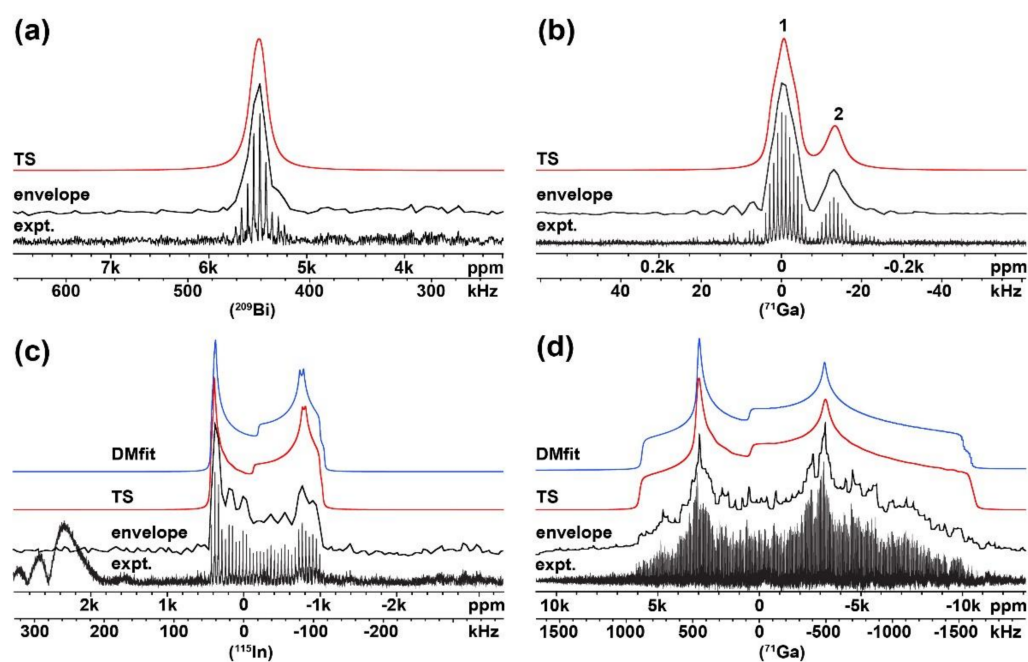


Figure 3. Experimental spikelets WURST-QCPMG NMR spectra (expt.), the envelope of the spectra defined by developed software (envelope), the fitting obtained from Bruker TopSpin (TS) software of: (a) ²⁰⁹Bi Cs₂AgBiBr₆; (b) ⁷¹Ga Ga(NO₃)₃·9H₂O; from Bruker TopSpin (TS) and DMfit (DMfit) software of: (c) ¹¹⁵In In(NO₃)₃·5H₂O; (d) ⁷¹Ga [Cl(Me)Ga(O^tBu)₂].

Initially, a relatively simple ²⁰⁹Bi NMR spectrum of the Cs₂AgBiBr₆ sample was examined. The profile of the experimental WURST-QCPMG NMR spikelets spectrum exhibited a symmetric lineshape with only one signal (Figure 3a and Figure S3). X-ray crystallographic data of the Cs₂AgBiBr₆ system (Figure S4) indicated a high symmetry (cubic) atomic arrangement around the Bi nucleus, as anticipated on the basis of the defined Fm-3m space group [37]. Simultaneously, the ²⁰⁹Bi nucleus is known to yield broad signals due to the considerable quadrupolar moment (eQ) and small values of the T_2 relaxation time constant, even in symmetric ²⁰⁹Bi site environments [38–40]. The combined effect of cubic symmetry and quadrupolar moment of Bi nuclei resulted in a relatively broad

symmetric spectral lineshape. NMR parameters fitted from the reconstructed lineshape are listed in Table 2. (The spectral envelope was fitted with a small C_Q value and a relatively large value of the line-broadening parameter, see Table 2 and Figure 3a.)

Table 2. Comparison of NMR parameters obtained from the experiment and from the periodic DFT calculations.

Compound	Investigated Nuclei	δ_{iso} (ppm)	σ_{iso} (ppm)	C_Q (MHz)	η_Q	Ω (ppm)	κ	α (deg)	β (deg)	γ (deg)	LB/GB (kHz)	
$\text{Cs}_2\text{AgBiBr}_6$ *	^{207}Bi	5517 (25)	4356	—* —*	—* —*	—* —*	—* —*	—* —*	—* —*	—* —*	—* 10.5/9.3	DFT Expt. ¹
$\text{Ga}(\text{NO}_3)_3 \cdot 9\text{H}_2\text{O}$	^{71}Ga (1)	−1 (5)	1680	1.5 1.0 (0.5)	0.76 0.7 (0.10)	68 51 (10)	0.76 0.7 (0.2)	144 128 (40)	32 50 (20)	310 293 (20)	— 1.5/1.2	DFT Expt. ¹
$\text{Ga}_{13}(\text{NO}_3)_{15}(\text{OH})_{24} \cdot 24\text{H}_2\text{O}$	^{71}Ga (2)	−80 (10)		0.9 (0.4)	0.2 (0.1)	33 (10)	0.4 (0.2)	14 (20)	138 (30)	177 (25)	3/0.5	Expt. ¹
$\text{In}(\text{NO}_3)_3 \cdot 5\text{H}_2\text{O}$	^{115}In	−80 (10)	3745	50.4	0.19	314	0.61	90	20	270	—	DFT
		−90 (10)		45.7 (0.5) 45.1 (0.5)	0.14 (0.03) 0.15 (0.03)	117 (25) 130 (25)	0.3 (0.1) 0.4 (0.1)	60 (15) 62 (15)	10 (10) 14 (10)	300 (30) 307 (30)	1.4/0 1.7/0	Expt. ¹ Expt. ²
$[\text{Cl}(\text{Me})\text{Ga}(\text{O}^t\text{Bu})_2]$	^{71}Ga	286 (23)	1408	37.8	0.53	491	0.59	174	10	274	—	DFT
		307 (24)		44.3 (0.4) 43.7 (0.4)	0.49 (0.05) 0.49 (0.05)	546 (55) 543 (50)	0.7 (0.2) 0.6 (0.2)	135 (40) 130 (35)	12 (10) 18 (10)	273 (20) 288 (25)	16.2/17.1 15.6/0	Expt. ¹ Expt. ²

$\delta_{iso} = (\delta_{11} + \delta_{22} + \delta_{33})/3$, $C_Q = eQV_{33}/h$, $\eta_Q = (V_{11} - V_{22})/V_{33}$, $\Omega = \delta_{11} - \delta_{33}$, $\kappa = 3(\delta_{22} - \delta_{iso})/\Omega$; Euler angles are defined in [36]; ¹ NMR parameters obtained using Bruker TopSpin software; ² NMR parameters obtained using DMfit software. * The values are zero by symmetry.

Somewhat more complex, the ^{71}Ga WURST-QCPMG NMR spikelets spectrum of the $\text{Ga}(\text{NO}_3)_3 \cdot 9\text{H}_2\text{O}$ sample showed two distinct peaks, which indicated two gallium sites with different local environments (Figure 3b and Figure S5). A subsequent XRPD analysis of the sample (Figure S6) confirmed the presence of two phases, namely, gallium nitrate hydrate ($\text{Ga}(\text{NO}_3)_3 \cdot 9\text{H}_2\text{O}$) and gallium nitrate hydrate hydroxide ($\text{Ga}_{13}(\text{NO}_3)_{15}(\text{OH})_{24} \cdot 24\text{H}_2\text{O}$). The presence of two distinct crystalline hydrates was the consequence of strict sample handling under an inert atmosphere (Ar). In laboratory conditions, only gallium nitrate hydrate ($\text{Ga}(\text{NO}_3)_3 \cdot 9\text{H}_2\text{O}$) was present. A relatively narrow and symmetric lineshape of the resulting ^{71}Ga NMR signals suggested small values of the quadrupolar coupling constant (C_Q) and CSA parameters. Thus, the ^{71}Ga NMR signals were fitted accordingly—using Lorentzian/Gaussian approximation (Table 2, Figure 3b). Moreover, the quantification of individual components was possible by the integration of the individual peaks as the resulting spectrum contained well-resolved signals. In this case, the molar ratio of 77% of ($\text{Ga}(\text{NO}_3)_3 \cdot 9\text{H}_2\text{O}$) and 23% of ($\text{Ga}_{13}(\text{NO}_3)_{15}(\text{OH})_{24} \cdot 24\text{H}_2\text{O}$) was found and confirmed by XRPD data.

As a next step, a system containing nuclei with a dominant quadrupolar contribution was selected. Here, the ^{115}In isotope was a suitable candidate due to its adequate sensitivity, gyromagnetic ratio and relatively easily resolved structural features, typical for all triel/icosagen elements. The experimental ^{115}In WURST-QCPMG NMR spectrum of $\text{In}(\text{NO}_3)_3 \cdot 5\text{H}_2\text{O}$ is depicted in Figure 3c and Figure S7. Clearly, the baseline of the experimentally obtained spikelets ^{115}In NMR spectrum was distorted due to the probe ringing. In order to remove this distortion, some part of the FID was cut (left-shifted); however, this resulted in a loss of intensity of the right shoulder of the signal (see Figure S8). Therefore, the initial spectrum with a full FID was used for further manipulation, and the option for the correction of the background (noise region) in the USS software was applied. A consequential spectral profile with an even background without any loss of intensity of the main signal was obtained (Figure 3c, envelope). Further, the NMR parameters (Table 2) were fitted using the Bruker TopSpin and DMfit software (Figure 3c, TS and DMfit). Additionally, the crystal structure of the investigated sample was confirmed by an X-ray diffraction phase analysis, verifying the presence of one pure phase (Figure S9).

Finally, the experimental ^{71}Ga WURST-QCPMG NMR spikelets spectrum of the $[\text{Cl}(\text{Me})\text{Ga}(\text{O}^t\text{Bu})_2]$ sample (Figure 3d, expt.) was acquired using the WURST-QCPMG experiment combined with the VOCS approach [16]. In order to obtain the whole powder pattern, seventeen sub-spectra had to be co-added. The resulting UWNMR spectrum was exceptionally wide, with ~ 2.5 MHz in breadth. Before transferring the obtained spectral

profile to the conventional software for fitting, the envelope was slightly smoothed (using the respective option in the USS software); see Figure 3d, envelope. Further, the spectral envelope was fitted as one ^{71}Ga site, in both the Bruker TopSpin and DMfit software (Figure 3d, TS and DMfit), and corresponding NMR parameters were obtained.

Experimental NMR parameters for all investigated samples ($\text{Ga}(\text{NO}_3)_3 \cdot 9\text{H}_2\text{O}$, $\text{Cs}_2\text{AgBiBr}_6$, $\text{In}(\text{NO}_3)_3 \cdot 5\text{H}_2\text{O}$, and $[\text{Cl}(\text{Me})\text{Ga}(\text{O}^t\text{Bu})_2]$) fitted with the aid of the USS software were compared with theoretical NMR values obtained from the periodic DFT calculations; see Table 2. The theoretical and experimental data showed good agreement in all cases. Furthermore, the corresponding XRPD patterns confirming the presence of individual compounds are listed in SI. It follows that the usability of the presented USS software for the fast and easy extraction of required NMR parameters was successfully verified.

3. Materials and Methods

3.1. Chemicals

Barium nitrate— $\text{Ba}(\text{NO}_3)_2$ —, barium carbonate— BaCO_3 —, barium chloride dihydrate— $\text{BaCl}_2 \cdot 2\text{H}_2\text{O}$ —, mercury (II) acetate— $\text{Hg}(\text{CH}_3\text{COO})_2$ —, gallium nitrate hydrate— $\text{Ga}(\text{NO}_3)_3 \cdot 9\text{H}_2\text{O}$ —and indium nitrate hydrate— $\text{In}(\text{NO}_3)_3 \cdot 5\text{H}_2\text{O}$ —were purchased from Sigma-Aldrich and used as received. Trimesitylaluminum— AlMe_3 —and Trimesityl-tetrahydrofuran-aluminum— $\text{AlMe}_3 \cdot \text{THF}$ —were prepared and handled as described in [30]. Lead diformate— $\text{Pb}(\text{HCOO})_2$ —was obtained according to the description provided in [35]. Cesium silver(I) bismuth(III) bromide— $\text{Cs}_2\text{AgBiBr}_6$ —was synthesized by the procedure described in the literature data [41]. Bis(μ_2 -*t*-butanolato)-dichloro-dimethyl-di-gallium— $[\text{Cl}(\text{Me})\text{Ga}(\text{O}^t\text{Bu})_2]$ (CAJXOC in CCDC database)—was prepared from the following chemicals: lithium bis(trimethylsilyl)amide solution in toluene (0.5 M), anhydrous toluene, and *t*-butanol, bought from Sigma-Aldrich, (St. Louis, MO, USA), gallium trichloride, ultra-dry, from Alfa Aesar (Haverhill, MA, USA). Argon 7.0 (Linde Gas; Prague, Czech Republic) was used as received. All procedures were conducted under argon atmosphere using Schlenk line techniques or glovebox. To prepare $[\text{Cl}(\text{Me})\text{Ga}(\text{O}^t\text{Bu})_2]$, we modified the two-step procedure described by Carmalt et al. [42]. Lithium bis(trimethylsilyl)amide solution (2.2 g, 25 ml, 0.5 M in toluene) was added through septum to suspension of GaCl_3 (1.1g GaCl_3 , 15 ml toluene) cooled at -78°C under argon atmosphere. The temperature was slowly allowed to rise and the mixture was refluxed overnight. Toluene was removed by argon flow, and residuum was vacuum-distilled. Crude white liquid $[\text{Me}(\text{Cl})\text{Ga}(\text{SiMe}_3)_2]$ was used in further steps without analysis. $[\text{Me}(\text{Cl})\text{Ga}(\text{SiMe}_3)_2]$ (1 g) was dissolved in toluene (15 ml) and *t*-butanol (3.6 mmol, 340 μL), refluxed overnight, then concentrated under vacuum. Resulting orange residuum was slowly sublimated using oil pump (10^{-2} torr) and heating mantel to obtain colorless crystals of $[\text{Cl}(\text{Me})\text{Ga}(\text{O}^t\text{Bu})_2]$. All prepared samples were stored in a glovebox with inert atmosphere (Ar).

3.2. Solid-State NMR

The ssNMR spectra were recorded at 11.7 T using a Bruker AVANCE III HD spectrometer. The 4 mm cross-polarization magic angle spinning (CP/MAS) probe was used. All spectra were recorded at static conditions using WURST-(Q)CPMG technique. In all measurements, 50 μs selective pulse was applied, and high-power ^1H decoupling (CW) was used to eliminate heteronuclear dipolar couplings. Dried samples were packed into ZrO_2 rotors and, subsequently, stored at room temperature in an inert atmosphere. All NMR spectra were processed using the Top Spin 3.5 pl2 software package, and spectral lines were simulated using the DMfit 2019 software [43]. Detailed experimental parameters and used external standards are listed in the SI (Tables S1 and S2, respectively). The spectra profiles based on the literature data (Figure 1, lit. data) were simulated in Bruker TopSpin software as fitting curves which corresponded to NMR parameters presented in respective scientific articles (see Table 1, [29,30,32–35]).

3.3. X-ray Powder Diffraction (XRPD)

Powder diffraction data were collected using the Bragg–Brentano reflection configuration on the powder diffractometer Empyrean of Panalytical (λ_{Cu} , $K_{\alpha} = 1.54184 \text{ \AA}$) that was equipped by a PIXcel3D detector. The phase analysis was performed in the Program HighScore connected with PDF 4+ and CSD databases. Crystallographic data of used samples are summarized in SI Table S3.

3.4. The Periodic Density Functional Theory (DFT) Calculations

The computational procedure was followed, which was most recently successfully applied by some of us to the ^{71}Ga NMR parameters in reference [44], where further details can be found. In short, it applies the plane wave DFT-based calculations as implemented in the CASTEP 16.1 code [45] to first optimize the periodic structures of investigated crystals, and, subsequently, predict their NMR parameters by applying the GIPAW method [46,47]. In all calculations, the PBE functional [48] was used, and relativistic effects were treated by the ZORA method [49]. The CASTEP settings were consistent with the “Fine” accuracy level of the Materials Studio [50].

3.5. Program Description and Data Processing

UWNMRspectralShape (USS) is a software with a graphical user interface (GUI) written in Java programming language (JDK 11.0) using an external JFreeChart library for plotting. The program was designed for fast and easy extraction of the final envelope of spikelets pattern of UWNMR spectra (for spectra to be processed properly they must be presented in magnitude (absolute value) mode; ‘mc’ command in TopSpin software) and its further transfer to conventional programs such as Bruker TopSpin and DMfit, or conversion into an ASCII file. The main interface of the software is shown in Figure 4. The GUI comprises three parts: (i) menu bar (top left), (ii) sidebar (left) and (iii) plot area (right). The menu bar contains options for conventional actions such as opening and saving files, showing the user guide, etc. The plot area displays the loaded NMR spectrum (Figure 4, black line). The sidebar is divided into sub-bars and contains radio-buttons for changing frequency units (ppm, Hz) and a text box indicating the basic transmitter frequency (ν_0 in MHz). The set of radio-buttons for switching between different processing options (after selecting an individual radio button, the corresponding option is enabled): (i) Finding spectral envelope, (ii) Smoothing mode, (iii) Background correction; buttons for Deleting spectral envelope, Cleaning up the plot area, Undo action, Zoom out and two buttons for Saving the final envelope in different formats.

Processing with USS software is intuitive and straightforward. After loading a UWNMR spikelets spectrum into the program, the sub-regions for creating spectral envelope need to be defined by a left mouse click in the plot area. These defined sub-regions and selected point(s) are then highlighted by vertical lines (see green lines in the inset magnification in Figure 4), and their positions are saved and used for subsequent processing. The coloring (green, magenta and gray) of the vertical lines depends on the processing option as follows:

Defining spectral envelope (green; see manual): Zoom in onto the spikelet signal(s) so that individual spikes are resolved. By clicking in between two consecutive spikes (as shown in Figure 4, where green lines are located), two sub-regions of the recorded NMR spectrum are defined. Then, the positions (on the x axis) of local maximum points in the defined sub-regions are automatically found using the “Linear search” algorithm:

1. The first point of the region is set as maximum (*max*)
2. FOR all points IN defined region DO (IF intensity of current point is higher than *max* THEN set current point as *max*)

As the distance between spikelets is constant (it depends only on experiment settings), the program automatically detects the local maximum of each spikelet. It builds the spectral envelope containing peak points of every spikelet and points from the noise region (which does not contain spikelets); see the red line in Figure 4. For several spectra, the results were

checked against essentially the same procedure implemented in a MATLAB[®] script that is described in the SI, Chart S1.

Smoothing mode (magenta; see manual): The generated spectral envelop (whole spectrum or defined region) can be smoothed by an implemented algorithm that averages the intensity of the local minimums relatively to the intensities of the neighboring points. This procedure slightly changes the intensity of the experimental data points in order to make the spectral profile look smoother; however, it has no impact on the obtained NMR parameters. This is performed using the following algorithm:

1. FOR all points IN whole profile (or defined region) DO (IF intensity of the current point is lower than intensities of both (closest) neighboring points THEN intensity of the current point is equal to an average value of intensities of the neighboring points)

Background correction (gray; see manual): The noise region(s) of the recorded NMR spectra with a distorted baseline need to be defined using a left mouse click. After selecting “Make background correction”, the intensity of noise points in the specified region are set to an average value ($\pm 10\%$) of the intensity between the first and the last points in the selected region (see as an example Figure 3c, expt. and envelope). This procedure uses the following algorithm:

1. An average intensity (*avg*) of the first and last points in the defined region is stored.
2. FOR all points IN the defined region DO intensity is equal to $avg \pm 10\%$.

Zoom: The left mouse button can be used for zooming in. Alternatively, the mouse wheel can zoom the spectrum in and out. When a certain area of the spectrum is zoomed in, it is possible to drag and move the spectrum (along both axes) using a combination of “Ctrl” and left mouse button. The “Zoom out” option can be used to set the zoom to the default position.

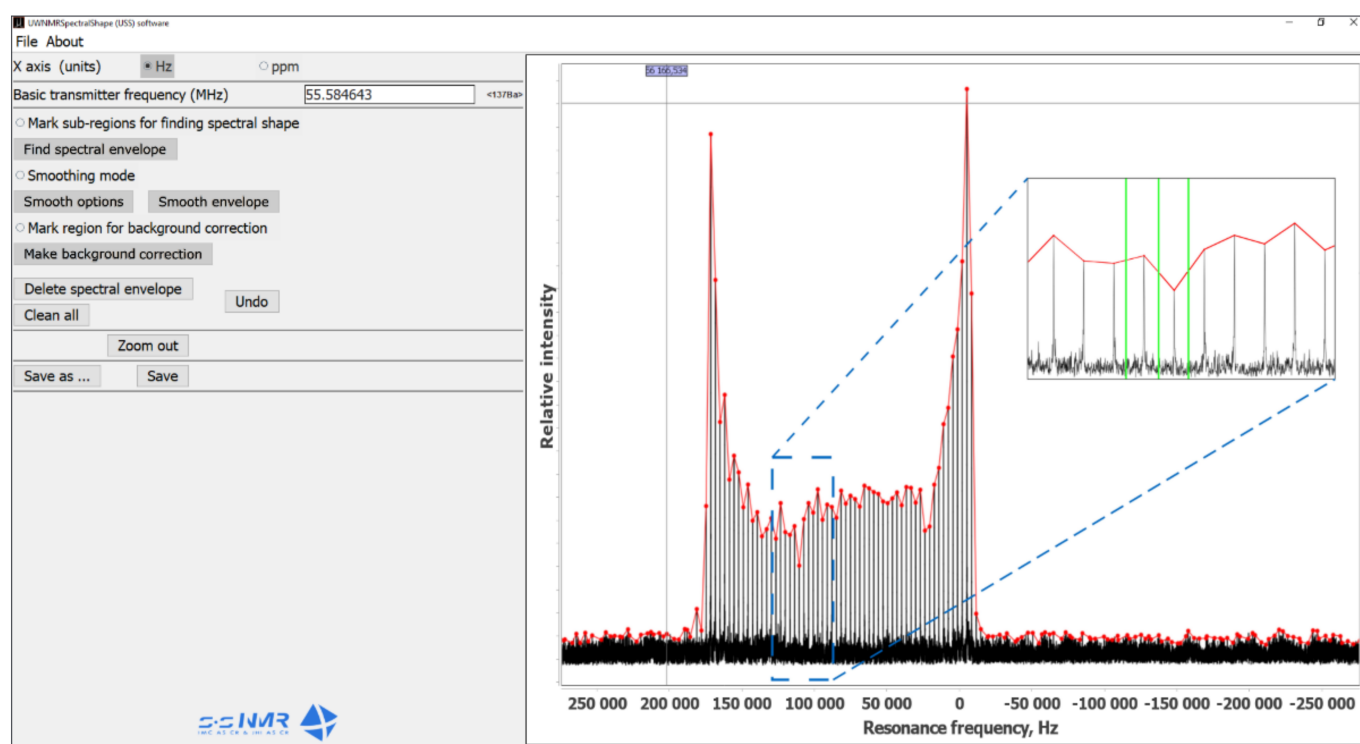


Figure 4. A screenshot of the main interface of UWNMR SpectralShape (USS) software.

A click of the right mouse button in the plot area leads to the appearance of a pop-up menu with plot options such as adding the title, editing axes and background, saving an image, etc. After processing the used UWNMR spectrum, the final continuous spectral line can be saved by clicking the “Save” or “Save as” button. The latter allows the user to

save the file in a chosen folder, whereas the “Save” button will save results to the original folder (where the initial/opened file is located). Finally, the spectrum obtained and saved in this way can be used for automatic fitting of NMR parameters, such as quadrupolar coupling constant (C_Q), asymmetry parameter (η_Q) and chemical shift anisotropy (CSA), etc., in conventional NMR programs. More processing details are given in the program user guide: About>>How to use program. The latest program version is available at <https://cutt.ly/evretIG> (accessed on 29 September 2021).

4. Conclusions

A new approach for obtaining NMR parameters using the developed software was proven to be both faster and more straightforward than the method based on the time-domain co-addition of spin echoes. Additionally, it gave more reliable results in comparison to the conventional approach using a manual simulation and fitting of the powder spikelets pattern. It was shown that the software is eminently suitable for processing all spikelets NMR spectra yielded by quadrupolar and spin- $1/2$ nuclei and allows the successful analysis of broad (hundreds kHz), as well as relatively narrow (tens kHz), signals. Finally, the subsequent quantification of well-resolved, distinct species can be determined using the traditional integration of individual peaks.

Supplementary Materials: The following are available online, Table S1: details of experimental parameters, Table S2: used external standards for NMR chemical shift referencing, Table S3: crystallographic data of the investigated compounds, Chart S1: description of a procedure for verifying the spectral shape, Figure S1: full experimental ^{137}Ba WURST-QCPMG NMR spectrum of BaCO_3 and the spectral profile obtained by the UWNMRsSpectralShape software, Figure S2: phase analysis of the measured powder diffraction pattern of BaCO_3 sample, Table S4: comparison of NMR parameters obtained by fitting spectral envelopes provided by different approaches for chosen model compounds, Figure S3: experimental ^{209}Bi WURST-QCPMG NMR spectrum of $\text{Cs}_2\text{AgBiBr}_6$, the spectrum profile obtained by the UWNMRsSpectralShape software, and experimental ^{209}Bi Hahn-echo spectrum, Figure S4: phase analysis of the measured powder diffraction of $\text{Cs}_2\text{AgBiBr}_6$ sample, Figure S5: experimental ^{71}Ga WURST-QCPMG NMR spectrum of $\text{Ga}(\text{NO}_3)_3$, the spectrum profile obtained by the UWNMRsSpectralShape software, and experimental ^{71}Ga Hahn-echo spectrum, Figure S6: phase analysis of the measured powder diffraction pattern of $\text{Ga}(\text{NO}_3)_3 \cdot 9\text{H}_2\text{O}$ sample, Figure S7: experimental ^{115}In WURST-QCPMG NMR spectrum of $\text{In}(\text{NO}_3)_3 \cdot 5\text{H}_2\text{O}$, the spectrum profile (with corrected background) obtained by the UWNMRsSpectralShape software, and experimental ^{115}In Hahn-echo spectrum, Figure S8: profiles obtained by the UWNMRsSpectralShape software of the ^{115}In WURST-QCPMG NMR spectrum of $\text{In}(\text{NO}_3)_3 \cdot 5\text{H}_2\text{O}$ processed with full and cut FID, Figure S9: phase analysis of the measured powder diffraction pattern of $\text{In}(\text{NO}_3)_3 \cdot 5\text{H}_2\text{O}$ sample.

Author Contributions: A.M.: software, validation, NMR measurement and analysis, manuscript preparation, funding; L.K.: concept, methodology, supervision, funding; S.A.: supervision, manuscript revision, J.B. and R.K.: formal analysis, W.N. and H.M.: sample preparation; J.C.: DFT calculations; funding; J.R.: XRPD measurements. All authors have read and agreed to the published version of the manuscript.

Funding: This work was supported by the Grant Agency of the Czech Republic (GA 19-05259S) and the Visegrad Scholarship No. 52010892.

Institutional Review Board Statement: Not Applicable.

Informed Consent Statement: Not applicable.

Data Availability Statement: All data are included in the article.

Acknowledgments: Computational resources were supplied by the project “e-Infrastruktura CZ” (e-INFRA LM2018140) provided within the program Projects of Large Research, Development and Innovations Infrastructures; and by the ELIXIR-CZ project (LM2015047), part of the international ELIXIR infrastructure.

Conflicts of Interest: The authors have declared no conflict of interest.

Sample Availability: Samples of the compounds are not available from the authors.

References

1. Pake, G.E. Nuclear Resonance Absorption in Hydrated Crystals: Fine Structure of the Proton Line. *J. Chem. Phys.* **1948**, *16*, 327–336. [[CrossRef](#)]
2. Pound, R.V. Nuclear Electric Quadrupole Interactions in Crystals. *Phys. Rev.* **1950**, *79*, 685–702. [[CrossRef](#)]
3. Smith, J.A.S. Nuclear quadrupole resonance spectroscopy. General principles. *J. Chem. Educ.* **1971**, *48*, 39–48. [[CrossRef](#)]
4. Mehring, M. *High Resolution NMR Spectroscopy in Solids*; Springer: Berlin, Germany, 1976.
5. Bakmutov, V.I. *Solid-State NMR in Materials Science: Principles and Applications*; Paramagnetic Effects in Solid-State NMR; CRC Press: Boca Raton, FL, USA, 2011; p. 191. ISBN 9781439869642.
6. Samoson, A.; Lippmaa, E.; Pines, A. High resolution solid-state N.M.R. Averaging of second-order effects by means of a double-rotor. *Mol. Phys.* **1988**, *65*, 1013–1018. [[CrossRef](#)]
7. Mueller, K.T.; Sun, B.Q.; Chingas, G.C.; Zwanziger, J.W.; Terao, T.; Pines, A. Dynamic-angle spinning of quadrupolar nuclei. *J. Magn. Reson.* **1990**, *86*, 470–487. [[CrossRef](#)]
8. Gan, Z. Satellite transition magic-angle spinning nuclear magnetic resonance spectroscopy of half-integer quadrupolar nuclei. *J. Chem. Phys.* **2001**, *114*, 10845–10853. [[CrossRef](#)]
9. Huguenard, C.; Taulelle, F.; Knott, B.; Gan, Z. Optimizing STMAS. *J. Magn. Reson.* **2002**, *156*, 131–137. [[CrossRef](#)] [[PubMed](#)]
10. Medek, A.; Harwood, J.S.; Frydman, L. Multiple-Quantum Magic-Angle Spinning NMR: A New Method for the Study of Quadrupolar Nuclei in Solids. *J. Am. Chem. Soc.* **1995**, *117*, 12779–12787. [[CrossRef](#)]
11. Schurko, R.W. Ultra-Wideline Solid-State NMR Spectroscopy. *Acc. Chem. Res.* **2013**, *46*, 1985–1995. [[CrossRef](#)]
12. Kobera, L.; Southern, S.A.; Rao, G.K.; Richeson, D.S.; Bryce, D.L. New Experimental Insight into the Nature of Metal–Metal Bonds in Digallium Compounds: J Coupling between Quadrupolar Nuclei. *Chem.—A Eur. J.* **2016**, *22*, 9565–9573. [[CrossRef](#)]
13. Kobera, L.; Southern, S.A.; Frost, J.M.; Bryce, D.L. Multinuclear solid-state magnetic resonance study of oxo-bridged diniobium and quadruply-bonded dimolybdenum carboxylate clusters. *Solid State Nucl. Magn. Reson.* **2017**, *84*, 20–27. [[CrossRef](#)]
14. Rhodes, H.E.; Wang, P.-K.; Stokes, H.T.; Slichter, C.P.; Sinfelt, J.H. NMR of platinum catalysts. I. Line shapes. *Phys. Rev. B* **1982**, *26*, 3559–3568. [[CrossRef](#)]
15. Bastow, T.J.; Smith, M.E. ⁹¹Zr NMR characterisation of phases in transformation toughened zirconia. *Solid State Nucl. Magn. Reson.* **1992**, *1*, 165–174. [[CrossRef](#)]
16. Massiot, D.; Farnan, I.; Gautier, N.; Trumeau, D.; Trokner, A.; Coutures, J.P. ⁷¹Ga and ⁶⁹Ga nuclear magnetic resonance study of β-Ga₂O₃: Resolution of four- and six-fold coordinated Ga sites in static conditions. *Solid State Nucl. Magn. Reson.* **1995**, *4*, 241–248. [[CrossRef](#)]
17. Hahn, E.L. Spin Echoes. *Phys. Rev.* **1950**, *80*, 580–594. [[CrossRef](#)]
18. Das, T.P.; Saha, A.K. Electric quadrupole interaction and spin echoes in crystals. *Phys. Rev.* **1955**, *98*, 516–524. [[CrossRef](#)]
19. Solomon, I. Multiple Echoes in Solids. *Phys. Rev.* **1958**, *110*, 61–65. [[CrossRef](#)]
20. Carr, H.Y.; Purcell, E.M. Effects of Diffusion on Free Precession in Nuclear Magnetic Resonance Experiments. *Phys. Rev.* **1954**, *94*, 630–638. [[CrossRef](#)]
21. Meiboom, S.; Gill, D. Modified Spin-Echo Method for Measuring Nuclear Relaxation Times. *Rev. Sci. Instrum.* **1958**, *29*, 688–691. [[CrossRef](#)]
22. Shore, S.E.; Ansermet, J.P.; Slichter, C.P.; Sinfelt, J.H. Nuclear magnetic resonance study of the bonding and diffusion of CO chemisorbed on Pd. *Phys. Rev. Lett.* **1987**, *58*, 953–956. [[CrossRef](#)]
23. Larsen, F.H.; Jakobsen, H.J.; Ellis, P.D.; Nielsen, N.C. Sensitivity-enhanced quadrupolar-echo NMR of half-integer quadrupolar nuclei. Magnitudes and relative orientation of chemical shielding and quadrupolar coupling tensors. *J. Phys. Chem. A* **1997**, *101*, 8597–8606. [[CrossRef](#)]
24. Lipton, A.S.; Wright, T.A.; Bowman, M.K.; Reger, D.L.; Ellis, P.D. Solid-state ⁶⁷Zn NMR spectroscopy in bioinorganic chemistry. Spectra of four- and six-coordinate zinc pyrazolylborate complexes obtained by management of proton relaxation rates with a paramagnetic dopant. *J. Am. Chem. Soc.* **2002**, *124*, 5850–5860. [[CrossRef](#)]
25. Bhattacharyya, R.; Frydman, L. Quadrupolar nuclear magnetic resonance spectroscopy in solids using frequency-swept echoing pulses. *J. Chem. Phys.* **2007**, *127*, 194503. [[CrossRef](#)]
26. Kupce, E.; Freeman, R. Adiabatic pulses for wideband inversion and broadband decoupling. *J. Magn. Reson. Ser. A* **1995**, *115*, 273–276. [[CrossRef](#)]
27. O'Dell, L.A.; Schurko, R.W. QCPMG using adiabatic pulses for faster acquisition of ultra-wideline NMR spectra. *Chem. Phys. Lett.* **2008**, *464*, 97–102. [[CrossRef](#)]
28. Tang, J.A.; O'Dell, L.A.; Aguiar, P.M.; Lucier, B.E.G.; Sakellariou, D.; Schurko, R.W. Application of static microcoils and WURST pulses for solid-state ultra-wideline NMR spectroscopy of quadrupolar nuclei. *Chem. Phys. Lett.* **2008**, *466*, 227–234. [[CrossRef](#)]
29. MacGregor, A.W.; O'Dell, L.A.; Schurko, R.W. New methods for the acquisition of ultra-wideline solid-state NMR spectra of spin-1/2 nuclides. *J. Magn. Reson.* **2011**, *208*, 103–113. [[CrossRef](#)]
30. Kobera, L.; Czernek, J.; Abbrent, S.; Mackova, H.; Pavlovec, L.; Rohlicek, J.; Brus, J. The Nature of Chemical Bonding in Lewis Adducts as Reflected by ²⁷Al NMR Quadrupolar Coupling Constant: Combined Solid-State NMR and Quantum Chemical Approach. *Inorg. Chem.* **2018**, *57*, 7428–7437. [[CrossRef](#)] [[PubMed](#)]

31. Hung, I.; Gan, Z. On the practical aspects of recording wide-line QCPMG NMR spectra. *J. Magn. Reson.* **2010**, *204*, 256–265. [[CrossRef](#)]
32. Hamaed, H.; Ye, E.; Udachin, K.; Schurko, R.W. Solid-State ^{137}Ba NMR spectroscopy: An experimental and theoretical investigation of ^{137}Ba electric field gradient tensors and their relation to structure and symmetry. *J. Phys. Chem. B* **2010**, *114*, 6014–6022. [[CrossRef](#)]
33. Bryce, D.L.; Bultz, E.B. Alkaline earth chloride hydrates: Chlorine quadrupolar and chemical shift tensors by solid-state NMR spectroscopy and plane wave pseudopotential calculations. *Chem.—A Eur. J.* **2007**, *13*, 4786–4796. [[CrossRef](#)]
34. Tang, J.A.; Masuda, J.D.; Boyle, T.J.; Schurko, R.W. Ultra-wide-line ^{27}Al NMR investigation of three- and five-coordinate aluminum environments. *ChemPhysChem* **2006**, *7*, 117–130. [[CrossRef](#)]
35. Švarcová, S.; Kočí, E.; Bezdička, P.; Garrappa, S.; Kobera, L.; Plocek, J.; Brus, J.; Štátný, M.; Hradil, D. Uncovering lead formate crystallization in oil-based paintings. *Dalt. Trans.* **2020**, *49*, 5044–5054. [[CrossRef](#)]
36. Power, W.P.; Wasylishen, R.E.; Mooibroek, S.; Pettitt, B.A.; Danchura, W. Simulation of NMR powder line shapes of quadrupolar nuclei with half-integer spin at low-symmetry sites. *J. Phys. Chem.* **1990**, *94*, 591–598. [[CrossRef](#)]
37. Slavney, A.H.; Hu, T.; Lindenberg, A.M.; Karunadasa, H.I. A Bismuth-Halide Double Perovskite with Long Carrier Recombination Lifetime for Photovoltaic Applications. *J. Am. Chem. Soc.* **2016**, *138*, 2138–2141. [[CrossRef](#)]
38. Hamaed, H.; Laschuk, M.W.; Tersikh, V.V.; Schurko, R.W. Application of solid-state ^{209}Bi NMR to the structural characterization of bismuth-containing materials. *J. Am. Chem. Soc.* **2009**, *131*, 8271–8279. [[CrossRef](#)]
39. Bieroń, J.; Pyykkö, P. Nuclear quadrupole moments of bismuth. *Phys. Rev. Lett.* **2001**, *87*, 133003. [[CrossRef](#)]
40. Leroy, C.; Bryce, D.L. Recent advances in solid-state nuclear magnetic resonance spectroscopy of exotic nuclei. *Prog. Nucl. Magn. Reson. Spectrosc.* **2018**, *109*, 160–199. [[CrossRef](#)]
41. Ji, F.; Huang, Y.; Wang, F.; Kobera, L.; Xie, F.; Klarbring, J.; Abbrent, S.; Brus, J.; Yin, C.; Simak, S.I.; et al. Near-Infrared Light-Responsive Cu-Doped $\text{Cs}_2\text{AgBiBr}_6$. *Adv. Funct. Mater.* **2020**, *30*, 2005521. [[CrossRef](#)]
42. Knapp, C.E.; Pugh, D.; McMillan, P.F.; Parkin, I.P.; Carmalt, C.J. Synthetic and structural studies of donor-functionalized alkoxy derivatives of gallium. *Inorg. Chem.* **2011**, *50*, 9491–9498. [[CrossRef](#)]
43. Massiot, D.; Fayon, F.; Capron, M.; King, I.; Le Calvé, S.; Alonso, B.; Durand, J.O.; Bujoli, B.; Gan, Z.; Hoatson, G. Modelling one- and two-dimensional solid-state NMR spectra. *Magn. Reson. Chem.* **2002**, *40*, 70–76. [[CrossRef](#)]
44. Kobera, L.; Havlin, J.; Abbrent, S.; Rohlicek, J.; Streckova, M.; Sopcak, T.; Kyselova, V.; Czernek, J.; Brus, J. Gallium Species Incorporated into MOF Structure: Insight into the Formation of a 3D Polycrystalline Gallium-Imidazole Framework. *Inorg. Chem.* **2020**, *59*, 13933–13941. [[CrossRef](#)]
45. Clark, S.J.; Segall, M.D.; Pickard, C.J.; Hasnip, P.J.; Probert, M.I.J.; Refson, K.; Payne, M.C. First principles methods using CASTEP. *Z. Krist.* **2005**, *220*, 567–570. [[CrossRef](#)]
46. Pickard, C.J.; Mauri, F. All-electron magnetic response with pseudopotentials: NMR chemical shifts. *Phys. Rev. B—Condens. Matter Mater. Phys.* **2001**, *63*, 2451011–2451013. [[CrossRef](#)]
47. Yates, J.R.; Pickard, C.J.; Mauri, F. Calculation of NMR chemical shifts for extended systems using ultrasoft pseudopotentials. *Phys. Rev. B* **2007**, *76*, 24401. [[CrossRef](#)]
48. Perdew, J.P.; Burke, K.; Ernzerhof, M. Generalized Gradient Approximation Made Simple. *Phys. Rev. Lett.* **1996**, *77*, 3865–3868. [[CrossRef](#)]
49. Yates, J.R.; Pickard, C.J.; Payne, M.C.; Mauri, F. Relativistic nuclear magnetic resonance chemical shifts of heavy nuclei with pseudopotentials and the zeroth-order regular approximation. *J. Chem. Phys.* **2003**, *118*, 5746–5753. [[CrossRef](#)]
50. BIOVIA Materials Studio. Dassault Systèmes, Vélizy-Villacoublay: Paris, France. Available online: <https://www.3ds.com/products-services/biovia/products/molecular-modeling-simulation/biovia-materials-studio/> (accessed on 29 September 2021).